The Plant Cell, Vol. 22: 3992–4008, December 2010, www.plantcell.org

A Recycling-Defective Vacuolar Sorting Receptor Reveals an Intermediate Compartment Situated between Prevacuoles and Vacuoles in Tobacco [W]

Ombretta Foresti,[a] David C. Gershlick,[a] Francesca Bottanelli,[a] Eric Hummel,[b,1] Chris Hawes,[b] and Jürgen Denecke[a,2]

[a] Centre for Plant Sciences, Faculty of Biological Sciences, University of Leeds, Leeds LS2 9JT, United Kingdom
[b] School of Life Sciences, Oxford Brookes, Oxford OX3 0BP, United Kingdom

Plant vacuolar sorting receptors (VSRs) display cytosolic Tyr motifs (YMPL) for clathrin-mediated anterograde transport to the prevacuolar compartment. Here, we show that the same motif is also required for VSR recycling. A Y612A point mutation in *Arabidopsis thaliana* VSR2 leads to a quantitative shift in VSR2 steady state levels from the prevacuolar compartment to the *trans*-Golgi network when expressed in *Nicotiana tabacum*. By contrast, the L615A mutant VSR2 leaks strongly to vacuoles and accumulates in a previously undiscovered compartment. The latter is shown to be distinct from the Golgi stacks, the trans-Golgi network, and the prevacuolar compartment but is characterized by high concentrations of soluble vacuolar cargo and the rab5 GTPase Rha1(RabF2a). The results suggest that the prevacuolar compartment matures by gradual receptor depletion, leading to the formation of a late prevacuolar compartment situated between the prevacuolar compartment and the vacuole.

INTRODUCTION

Protein transport to plant vacuoles occurs via the secretory pathway, a complex network of cell compartments that maintain unique steady state compositions of lipids and proteins despite a constant influx/efflux of biomolecules through vesicular transport (Jurgens, 2004). Some of these compartments form cross-junctions between biosynthetic and endocytic traffic (Foresti and Denecke, 2008; Otegui and Spitzer, 2008), making the analysis of the various dynamic equilibria particularly challenging.

Selective transport of soluble proteins is mediated by membrane-spanning receptor proteins that contain two domains facing opposite sides of the membrane. The lumenal domain mediates the binding of ligands in the donor organelle and their subsequent release in the acceptor organelle. The cytosolic domain mediates integration of receptors into appropriate transport carriers at both the donor and acceptor membranes. Receptors, membranes, and vesicle fusion machinery are recycled between organelles (Bonifacino and Glick, 2004), which allows few receptor molecules to transport many cargo molecules (Bonifacino and Rojas, 2006; Pfeffer, 2007). Recycling is also thought to protect receptors from proteolysis when they play a role in protein transport to lytic environments. The VPS10 gene product in yeast and the mammalian mannose-6-phosphate receptor recycle from nonlytic prevacuolar/prelysosomal intermediate compartments to avoid exposure to the lytic environment of the vacuoles (Seaman, 2005).

The first member of the plant vacuolar sorting receptor (VSR) family was identified in *Pisum sativum* as a type I membrane spanning protein of 80 kD (BP80), using clathrin-coated vesicles (CCVs) as starting material and vacuolar sorting signals as affinity bait (Kirsch et al., 1994). Plant VSRs have the same topology as the mannose-6-phosphate receptor in mammals and the VPS10 gene product in yeast. However, they show highest steady state levels in the prevacuolar compartment (PVC), rather than in the cargo donor compartment because in plants the recycling reaction is rate limiting (Tse et al., 2004; daSilva et al., 2005).

Plant VSRs have a large lumenal ligand binding domain and a short cytosolic tail displaying a conserved YMPL sequence. This consensus sequence fits into the well-known category of YxxΦ motifs in which Y is always Tyr, X is any amino acid, and Φ represents a bulky hydrophobic amino acid. YxxΦ is more commonly known for its role in clathrin-mediated endocytosis from the plasma membrane, but it is also known to be involved in the biosynthetic transport of proteins to lysosomes/vacuoles from the *trans*-Golgi network (TGN) (Ohno et al., 1995; Höning et al., 1996; Bonifacino and Dell'Angelica, 1999). Consistent with this role, the YMPL sequence of *Arabidopsis thaliana* VSRs was shown to be essential for recruitment of clathrin adaptors in vitro (Happel et al., 2004) and VSR sorting in vivo (daSilva et al., 2006).

Several key questions about VSR function remain unanswered (Foresti and Denecke, 2008). It is not firmly established if CCVs harboring cargo-loaded VSRs exit directly from the Golgi stacks (Hillmer et al., 2001; Happel et al., 2004) or if VSRs first accumulate in the TGN, also known as partially coated reticulum

[1] Current address: Institute of Cell Biology, University of Bayreuth, LB1/B1, 95440 Bayreuth, Germany.
[2] Address correspondence to j.denecke@leeds.ac.uk.
The author responsible for distribution of materials integral to the findings presented in this article in accordance with the policy described in the Instructions for Authors (www.plantcell.org) is: Jürgen Denecke (j.denecke@leeds.ac.uk).
[W] Online version contains Web-only data.
www.plantcell.org/cgi/doi/10.1105/tpc.110.078436

(Dettmer et al., 2006; Lam et al., 2007a, 2007b), a structure that is physically separated from the Golgi stacks in plants (Uemura et al., 2004; Foresti and Denecke, 2008). It is also unclear how VSRs and their cargo segregate from each other and how the cargo ultimately reaches the vacuole. Components of the plant retromer complex have been identified in recent years, but their subcellular localization and their mode of action in receptor recycling is controversial (Oliviusson et al., 2006; Shimada et al., 2006; Jaillais et al., 2007; Phan et al., 2008; Yamazaki et al., 2008; Niemes et al., 2010).

To address these questions, we studied VSR traffic directly to identify sorting motifs and pathways. The *Arabidopsis* VSR isoform at2g14720 (annotated as VSR2 in The Arabidopsis Information Resource) was chosen as the model as it bears the highest homology to the first plant VSR (BP80) purified from CCVs (Kirsch et al., 1994, 1996). We used a green fluorescent protein (GFP)-VSR2 fusion that no longer binds ligands but carries the transmembrane domain and the cytosolic tail of the receptor (daSilva et al., 2005). This fusion was shown to cycle through the same pathway as the full-length receptor, and it competes with endogenous receptors for transport machinery at the rate-limiting recycling step from the PVC (daSilva et al., 2005). As a consequence, endogenous receptors are degraded in the vacuole, and induced secretion of soluble vacuolar cargo can be measured quantitatively in response to competitor dosage. This assay provided an efficient way to screen mutants in the cytosolic tail because defects at any point of the VSR transport cycle would lead to reduced competition (daSilva et al., 2006). In particular, two mutations in the YMPL sequence (Y612A and L615A) were shown to reduce drastically in vivo competition by GFP-VSR2 (daSilva et al., 2006).

Here, we show that the Y and Φ mutations of the same YxxΦ motif both interfere with in vivo competition, but they have opposite effects on the actual fate of the VSRs, which sheds light on the full transport cycle of the receptor. The results show that both the arrival and the retrieval of VSRs from the PVC are signal dependent and that the PVC is not the last organelle in the biosynthetic route to the vacuole. A PVC maturation model is presented that may explain how the plant secretory pathway ensures that only cargo but not receptors reach the vacuole.

RESULTS

The YXXΦ Motif of Plant VSRs Exhibits a Bipartite Structure

The Y612A and L615A mutants showed the strongest phenotype in the initial screen for receptor targeting mutants (daSilva et al., 2006). To compare these two in a more quantitative manner, we measured induced secretion of vacuolar cargo in response to increasing concentrations of the two truncated receptor constructs (Figure 1A). As vacuolar cargo, we used the barley (*Hordeum vulgare*) enzyme α-amylase fused to a short peptide comprising the vacuolar sorting signal of sweet potato (*Ipomoea batatas*) sporamin (Pimpl et al., 2003). Tobacco leaf protoplasts were transfected with a constant amount of plasmid encoding the cargo, together with a dilution series of plasmid encoding the competitor. After incubation of the cell suspensions to allow for gene expression and protein transport, cells and medium were separated quantitatively, followed by measurement of the enzymatic activity of the reporter (Amy-spo) in the two fractions. The secretion index was then calculated as ratio of activities (medium/cells) to facilitate instant comparisons. Figure 1A shows the secretion index without competitor (first lane) and with increasing concentrations of either wild-type GFP-VSR2 (white bars), the Y612A mutant (black bars), or the L615A mutant (gray bars). Cells were also analyzed for the amounts of competitor (Figure 1B) to verify that the three recombinants were expressed at adequate levels for direct comparisons. The dose–response analysis illustrates that the two point mutations cause a similar decrease in the ability of GFP-VSR2 to induce Amy-spo secretion.

Since the in vivo competition by truncated receptor (GFP-VSR2) saturates the recycling route rather than the anterograde step, introducing more full-length receptors is sufficient to restore vacuolar sorting under these conditions (daSilva et al., 2005). We thus performed a complementation assay by cotransfecting a constant amount of plasmids encoding Amy-spo and GFP-VSR2 together with increasing concentrations of plasmids encoding the full-length VSR2 wild type or the two mutants. Figure 1C shows the secretion index of the vacuolar cargo Amy-spo and Figure 1D is a protein gel blot from cell extracts to monitor the amount of coexpressed full-length VSR2 and its two mutant derivatives. The results show that full-length VSR2 counteracts the effect of the competitor as seen by a dose-dependent reduction of Amy-spo secretion (white bars). As expected from previous results, full-length VSR2(Y612A) further aggravates the effect of the competitor (black bars) as it mistargets to the plasma membrane and carries vacuolar proteins en route (daSilva et al., 2006). In sharp contrast, the full-length VSR2(L615A) mutant retains the wild-type ability to restore vacuolar sorting and leads to a similar dose-dependent reduction of Amy-spo secretion (gray bars) compared with wild-type VSR2 (white bars). Although both mutations lie within the same YXXΦ motif, they show opposite phenotypes in the complementation assay.

We explored these findings further in tobacco leaf epidermis cells by live bioimaging of the three GFP-VSR2 fusions after *Agrobacterium tumefaciens*–mediated leaf transformation. To monitor inhibition of vacuolar sorting in situ, we coexpressed these GFP-VSR2 fusions with a soluble vacuolar cargo derived from Aleu-GFP (Di Sansebastiano et al., 2001) in which the GFP portion was replaced by red fluorescent protein (RFP), which is readily fluorescent at acidic pH typical for plant vacuoles (Hunter et al., 2007).

Figure 2A shows expression of Aleu-RFP alone, displaying diffuse fluorescence in the large central vacuole that represents the majority of lower leaf epidermis cells. In addition, small fluorescent punctate structures can be seen at the cell periphery, a thin layer of cytosol between the vacuolar membrane and the plasma membrane. These punctate structures (white arrows) are best appreciated when focusing on the cell surface (cortex) to image the thin cytosol layer that hosts these organelles (right panel).

As expected, coexpression of Aleu-RFP with GFP-VSR2 leads to missorting of Aleu-RFP to the apoplast (Figure 2B). By contrast, coexpression with the two mutants GFP-VSR2(Y612A) (Figure 2C) and GFP-VSR2(L615A) (Figure 2D) had no influence on the vacuolar marker. This was in contrast with the biochemical

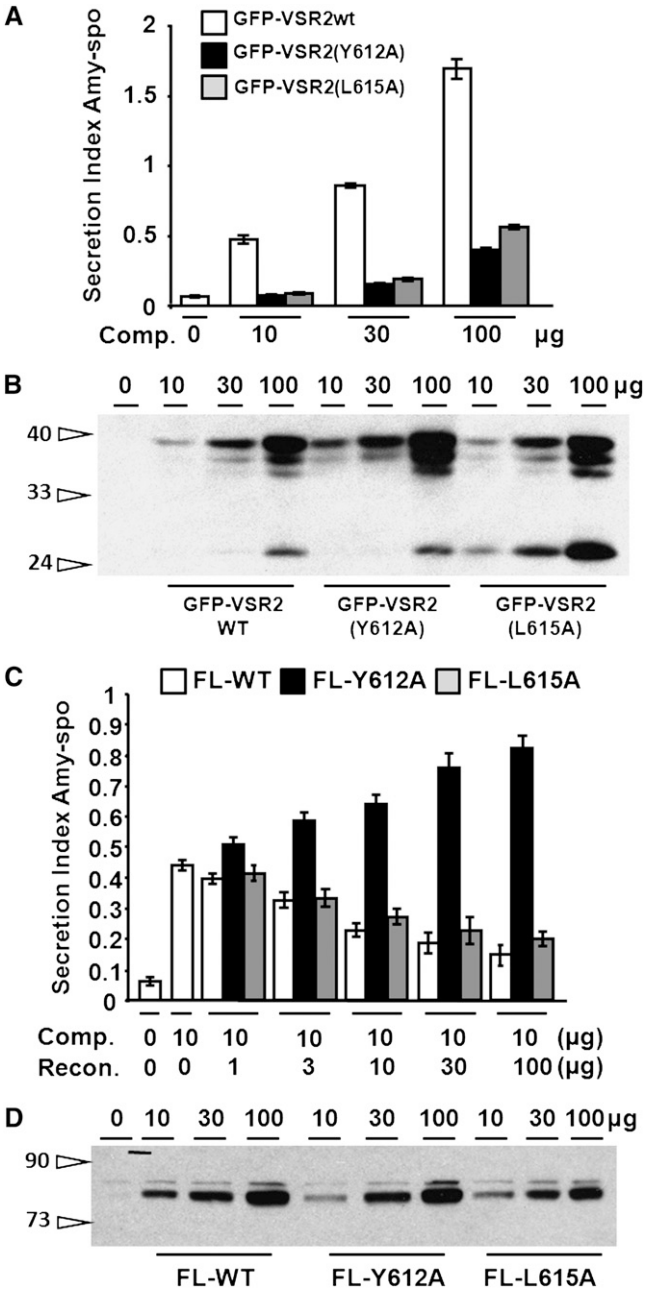

Figure 1. In Vivo Receptor Competition/Reconstitution Assays.

(A) Quantitative transient expression experiment with tobacco leaf protoplasts transfected with a constant amount of plasmid encoding vacuolar cargo (Amy-spo) together with increasing concentrations of plasmid encoding the competitor GFP-VSR2 (white bars) or its two mutant derivatives (Y612A shown in black bars or L615A shown in gray bars). The secretion index, which is the ratio of extracellular to intracellular amylase activity, is shown as a function of the amount of competitor (Comp.; plasmid concentrations given in micrograms). Error bars are the standard deviations calculated from five independent transfection experiments. Notice that the two point mutations strongly reduce in vivo competition compared with the wild-type (wt) competitor.

(B) Protein gel blot of a representative sample of cell extracts from the data set in **(A)** using rabbit anti-GFP.

(C) Reconstitution assay using the same model system as in **(A)**, but in addition to a constant amount of cargo and of competitor GFP-VSR2 (Comp.), we cotransfected an increasing concentration of plasmid encoding either the full-length (FL) receptor VSR2 or its two mutant derivates (FL-Y612A or FL-L615A) to test reconstitution of vacuolar sorting (Recon.). Bars are annotated as in **(A)**. Notice that the FL-Y612 mutant aggravates the effect of the competitor, while the FL-L615A mutant reconstitutes vacuolar sorting.

(D) Protein gel blot of a representative sample of cell extracts from the data set in **(C)** using rabbit antiserum raised against the lumenal portion of VSR2 (Tse et al., 2004).

assay in protoplasts, which revealed a weak residual in vivo competition by both mutants (Figure 1A) due to multicopy expression from plasmid-borne genes. This was below the detection limit in the in situ assay using the infiltrated tobacco leaves (Figure 2) that harbor stable genomic integrations, yielding much weaker expression levels of the three VSR2 fusions. These were comparable to endogenous VSR levels as seen from protein gel blots probed with an antibody raised against the cytosolic tail of VSR2 (Tse et al., 2004). Interestingly, the green fluorescent pattern of the two GFP-VSR2 mutants themselves is very different. The Y612A mutant is found at the periphery of the cell and in punctae (Figure 2C), while the L615A mutant is found mainly to label punctate structures (Figure 2D), similar to the wild-type construct (Figure 2B).

We then tested the effect of the point mutations on the untagged full-length receptor and repeated the in situ coexpression with the vacuolar cargo Aleu-RFP. Equivalent expression of the full-length VSR2 constructs was routinely verified by immunoblotting using anti-VSR2 antibodies raised against the lumenal VSR2 domain (Tse et al., 2004) on extracts from the infiltrated leaf areas used for microscopy. As expected, coexpression of the Y612A mutant of the full-length receptor induced the secretion of vacuolar cargo, as documented by the noticeable redistribution of Aleu-RFP from the central vacuole to the apoplast in the majority of cells analyzed (Figure 2E, middle panel). By contrast, the L615A mutant showed no such effect and allowed normal vacuolar deposition of Aleu-RFP, as with wild-type VSR2 (Figure 2E, left and right panels).

Together, the results suggest that although the Y and Φ mutations both reduce the ability of the truncated receptor construct GFP-VSR2 for in vivo competition, they must affect different steps in the VSR transport cycle.

The YxxΦ Leu Mutant Shows Increased Leakage to the Vacuole

The earlier observed partial mistargeting of the Y612A mutant to the plasma membrane suggested a defect in anterograde transport (daSilva et al., 2006). By contrast, the L615A mutant is not detected at the plasma membrane and could thus be defective in the recycling step. The properties of the GFP-VSR fusion provide a biochemical tool to test this directly. When GFP-VSR2 saturates the recycling machinery and leaks to the vacuole, the GFP portion is cleaved, resulting in a stable lower molecular weight

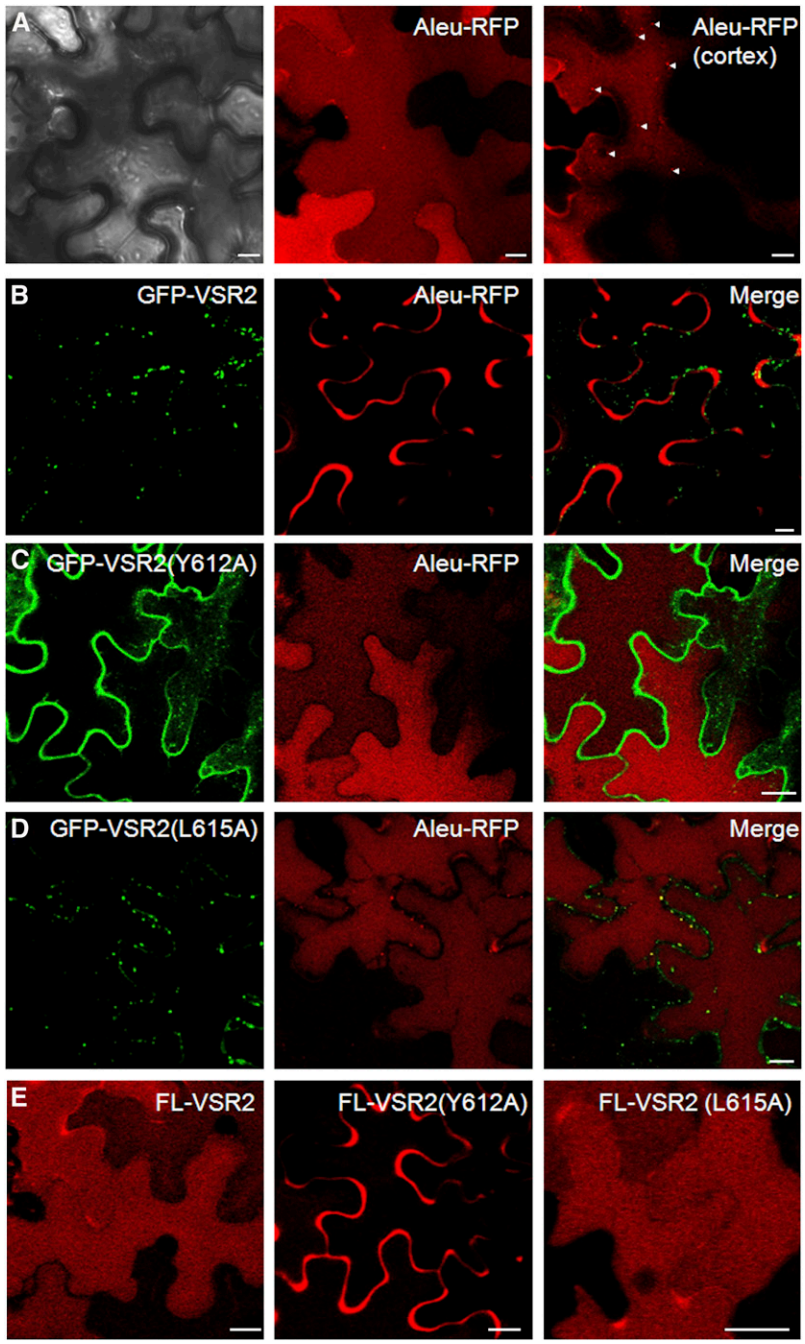

Figure 2. In Situ Competition Assays.

(A) Tobacco leaf epidermis cells expressing soluble vacuolar cargo Aleu-RFP after *Agrobacterium*-mediated cell transformation, showing a typical epidermis cell in bright field (left) and red fluorescence in dark field (middle). Typically, the vacuole lumen occupies most of the cell volume and shows diffuse red fluorescence. At left, the same cell is imaged with the focal plane on the cell surface (cortex) containing a portion of vacuole lumen with diffuse red fluorescence and a thin layer of cytosol with fluorescent mobile punctate structures (white arrow heads) representing Aleu-RFP in transit to the vacuole. Bar = 20 μm.

(B) to **(D)** In situ receptor competition assay using the same cell types as in **(A)** but the vacuolar cargo Aleu-RFP was cotransfected with the competitor GFP-VSR2 (wt) **(B)** or its mutant derivatives Y612A **(C)** or L615A **(D)**. Redistribution of vacuolar red fluorescence to the extracellular matrix is prominent only when the wild-type construct is used as competitor. Notice that the L615A mutant does not label the cell surface/apoplast, in contrast with the Y612A mutant. Bar = 20 μm.

(E) Effect of full-length (FL) untagged VSR2 and mutant derivatives (FL-Y612A and FL-L615A) on Aleu-RFP sorting in tobacco leaf epidermis cells. Notice that the FL-Y612A mutant inhibits vacuolar sorting in a dominant manner as observed before using biochemical assays (Figure 1C; see daSilva et al., 2006). By contrast, the FL-L615A mutant does not impair vacuolar sorting. Bar = 20 μm.

degradation intermediate, termed GFP core (daSilva et al., 2005, 2006). Figure 1B shows that under saturating expression levels, GFP-VSR2 precursor is enriched for the Y612A mutation, while GFP core formation is increased for the L615A mutation. Given the lower expression levels of recombinant proteins after stable DNA integration in the genome of tobacco epidermis cells (Figure 2), we now tested in this expression system if GFP-VSR2 processing is also differentially affected by the two mutations.

Infiltrated leaf areas taken from experiments illustrated in Figures 2B to 2D were extracted and analyzed by immunoblotting. Figure 3A confirms that in comparison to wild-type GFP-VSR2, the Y612A mutant shows more full-length precursor and reduced GFP core levels, consistent with the established anterograde transport defect leading to reduced leakage to the vacuole (daSilva et al., 2006). In sharp contrast, the L615A mutant behaves in the opposite manner and shows less full-length precursors and drastically increased GFP core levels. This suggests increased leakage to the vacuole and, thus, a defect in recycling.

Furthermore, expression of GFP-VSR2(Y612A) is characterized by formation of an alternative processed fragment (APF), consistent with earlier observations on VSR2(Y612A) linked to its mistargeting to the cell surface (daSilva et al., 2006). This APF band was not observed for the L615A mutant, similar to the wild-type fusion. Together, the results provide convincing evidence for differential processing of the two mutants. It should be noted that extracts from washed protoplasts (Figure 1B) do not show evidence for Y612A-induced APF formation. This is due to the fact that the leaf extracts contain both protoplasts and apoplast, unlike washed protoplasts from which secreted material has been removed with the culture medium (daSilva et al., 2006). In addition, compared with the protoplast transient expression results (Figure 1B), the differential effect of the two mutations on the appearance of the GFP core fragment is much more obvious in transformed leaves due to lower expression (Figure 3A). For these reasons, all further experiments on the influence of the two mutations on VSR2 sorting were conducted with the leaf epidermis expression system.

GFP fluorescence in plant vacuoles is quenched due to low pH (Tamura et al., 2003), and diffuse green fluorescence emitted by the GFP core is below the detection limit in Figure 2D (right panel). To allow visual appreciation of increased vacuolar leakage, we reconstructed the three fluorescent VSR2 fusions as RFP fusions. Figure 3B shows that vacuolar RFP fluorescence could not be detected for wild-type RFP-VSR2 and RFP-VSR2 (Y612A). By contrast, the vacuolar lumen of cells expressing RFP-VSR2(L615A) was very prominent. Given the large volume of the plant vacuole in which processed soluble RFP is diluted, the result provides a convincing visual display of increased vacuolar leakage, consistent with increased GFP core formation in Figures 1B and 3A.

The YxxΦ Tyr Mutant Accumulates in the TGN

To study the subcellular distribution of GFP-VSR2 and its mutant derivatives, we took advantage of the properties of the leaf epidermis system to obtain high-quality imaging data. Rather than focusing on the center of the cells to monitor fluorescence in the central vacuole and the apoplast at low magnification (Figures 1 and 2), we imaged the cytosol at the cell cortex at high magnification. Under these conditions, cell surface fluorescence is outside the focal plane, which permits analysis of punctate cytosolic structures, such as Golgi stacks, TGNs, and PVCs, within a thin layer of cytosol sandwiched between the plasma membrane and the vacuolar membrane. To quantify and display colocalization results from many images in a statistically meaningful and transparent manner, we performed correlation analysis using the Pearson-Spearman correlation (PSC) plug-in for ImageJ (French et al., 2008). This involved manual masking of punctate signals on a minimum of 20 independent images, containing at least 400 individual punctae in total for each coexpression experiment. The software considers individual pixels, which helps to distinguish partially overlapping signals from true colocalization (French et al., 2008).

Control experiments confirmed that wild-type GFP-VSR2 showed no significant colocalization with either the Golgi marker ST-RFP (Figure 4A) or the TGN marker yellow fluorescent protein (YFP)-Syp61 (Figure 4B) in this expression system. Each row of Figure 4 displays a representative fluorescent image of the test object GFP-VSR2, shown in green, the coexpressed organelle marker, shown in red, and the merged image. The rightmost panel of each row shows a scatterplot resulting from all images analyzed for each combination, in addition to the calculated Pearson (r_p) and Spearman (r_s) correlation coefficients. The plots clearly visualize two completely distinct populations of either green pixels representing wild-type GFP-VSR2 or red pixels corresponding to the Golgi or TGN markers, and the correlation coefficients are below zero in both cases. By contrast, the two wild-type receptor fusions GFP-VSR2 and RFP-VSR2 showed strong colocalization with each other (Figure 4C), giving rise to a typical diagonal scatterplot and high correlation values. This illustrates that the nature of the fluorescent protein does not influence localization per se, allowing us to use wild-type RFP-VSR2 as a common denominator for normal receptor localization in the PVC for comparisons with the two mutants.

We have shown previously that GFP-VSR2(Y612A) is partially mistargeted to the plasma membrane and partially accumulates in an unidentified post-Golgi compartment (daSilva et al., 2006). To identify the latter, we repeated the experiment in Figure 4 but using GFP-VSR2(Y612A) as test object with the three punctate organelle markers. The coexpression experiment with the Golgi marker ST-RFP (Figure 5A) reveals two distinct populations of punctae, either red signals clustering near the *x* axis or green signals clustering near the *y* axis. Negative Pearson and Spearman *r* values indicate a negative signal correlation. This confirms in leaf epidermis cells that the Y612A mutation does not cause Golgi retention (daSilva et al., 2006). In sharp contrast, the coexpression experiments with the TGN marker revealed a diagonal pattern of predominantly yellow color (Figure 5B). Both Pearson and Spearman *r* values are high, indicating strong colocalization.

When using wild-type RFP-VSR2 as PVC marker, only a partial overlap was detected with GFP-VSR2(Y612A) (Figure 5C). Partial overlap is due to the fact that the Y612A mutation does not completely block progress to the PVC. However, the scatterplot of individual pixels shows segregation of predominantly green or red signals. Even though pure visual inspection of individual punctate structures reveals that a large proportion of the

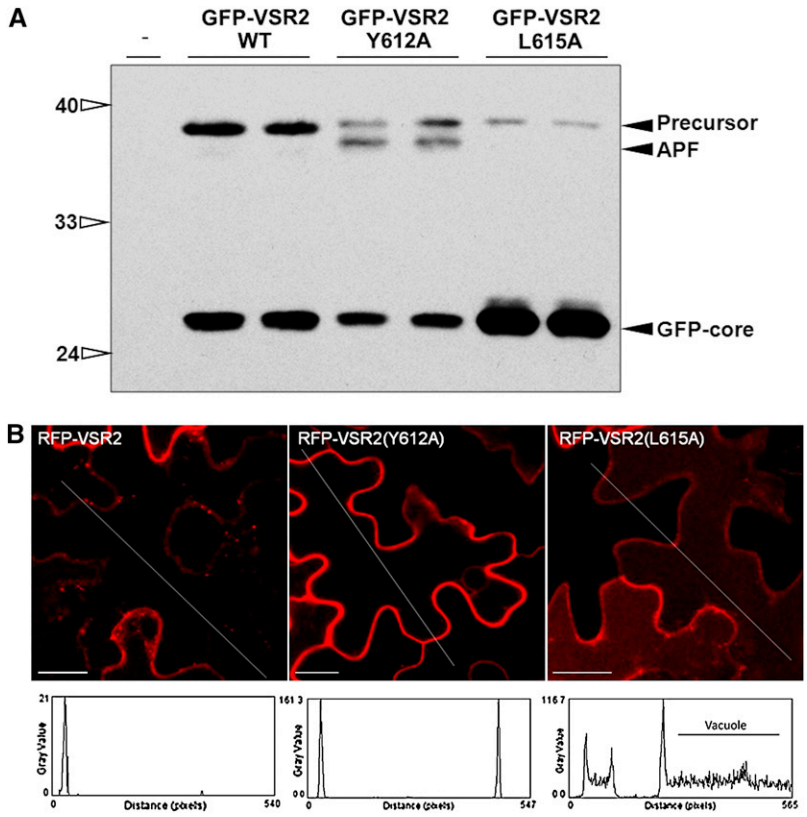

Figure 3. Biochemical and in Situ Assays to Document Vacuolar Leakage.

(A) Transformed leaf sections collected from experiments presented in Figures 2B to 2D were extracted in the presence of detergent to monitor membrane spanning GFP-VSR2 precursor as well as the soluble vacuolar degradation product termed GFP core (daSilva et al., 2005) and the larger APF that is typical for receptor mistargeting to the plasma membrane (daSilva et al., 2006). As a control, a leaf extract from untransformed leaves was used (−). The sizes of molecular weight markers are indicated in kilodaltons. Notice that GFP core formation is decreased for Y612A and increased for L615A and that only the Y612A mutant displays the APF. WT, wild type.

(B) Tobacco leaf epidermis cells expressing RFP-VSR2 (wt) or its two mutant derivatives (Y612A or L615A). Notice that diffuse vacuolar fluorescence is only noticeable for the L615A mutant. Line scans of cell images are indicated below each graph. Bar = 20 μm.

structures are yellow, the distribution of the intensity of the two signals is not correlated. Pearson and Spearman correlation coefficients were found to be very low and in stark contrast with the strong colocalization of the two wild-type fusions GFP-VSR2 and RFP-VSR2 with each other (Figure 4C). Together, the data show that the effect of the Y612A point mutation is a quantitative shift of steady state levels from the PVC to the TGN (cf. Figures 4C and 5C) and illustrate how quantification using PSC correlation on a large number of images yields more information than visual inspection of single images.

To rule out transient expression artifacts or unexpected features of fluorescent protein fusions, the results were confirmed at the ultrastructural level with the help of transgenic plants expressing full-length VSR2(Y612A) and wild-type VSR2 (daSilva et al., 2006). To probe ultrasections of tobacco root cells, we used a polyclonal anti-VSR2 antibody (Tse et al., 2004) that shows little or no cross-reaction with endogenous tobacco VSRs (daSilva et al., 2006). Figure 6A shows that the Y612A mutant accumulates mainly at the *trans*-face of the Golgi stacks in a physically separated extra-Golgi structure of irregular shape, earlier described as TGN (Dettmer et al., 2006). No labeling of PVCs with the typical multivesicular appearance was found in sections from this transgenic plant, although partial leakage of VSR2(Y612A) to PVC structures may have simply been below the detection limit. By contrast, PVC labeling was often found for wild-type VSR2 (Figure 6B), consistent with previous studies (Tse et al., 2004). Figure 6C shows the number of gold particles observed labeling the Golgi cisternae, the TGN, or the PVC. The statistical resolution of immunogold labeling experiments is lower compared with the PSC correlation from a much larger number of fluorescent structures (Figures 4 and 5), yet the experiment clearly supports the fact that subcellular localization of VSR2(Y612A) is shifted from PVC to TGN structures compared with the wild-type receptor.

The YxxΦ Leu Mutant Transits through a Late PVC

While the Y612A mutant showed reduced leakage to the vacuole, the L615A mutant revealed a stronger tendency for vacuolar degradation (Figure 3), suggesting a recycling defect. To gain

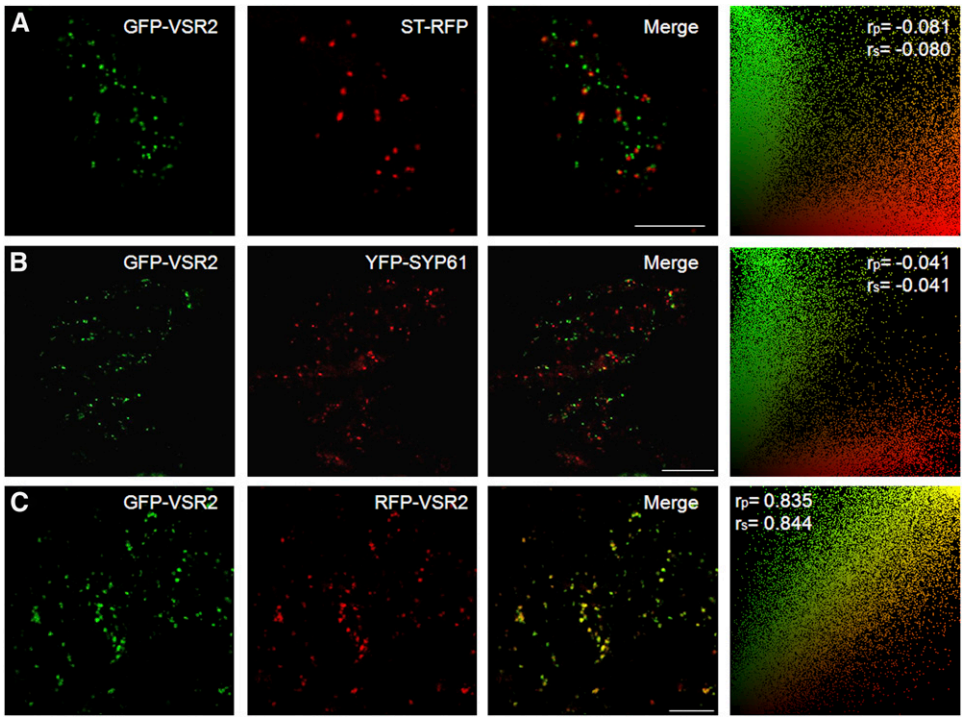

Figure 4. Quantitative Colocalization Analysis for GFP-VSR2 with Known Organelle Markers.

Tobacco leaf epidermis cells were transformed by *Agrobacterium* infiltration to express GFP-VSR2 with the Golgi marker ST-RFP **(A)**, the TGN-marker YFP-SYP61 **(B)**, and the PVC marker RFP-VSR2 **(C)**. Shown are typical examples of fluorescent images captured from the epidermis cell cortex of each combination. The scatterplots at the right-hand side of each row were obtained after manual masking of a minimum of 400 individual punctae from at least 20 independent cell images. The associated Pearson or Spearman *r* values indicate the level of colocalization ranging from +1 for perfect colocalization to −1 for negative correlation. Notice that the Golgi and TGN markers show negative correlation coefficients with GFP-VSR2 and distribute into distinct red or green structures, while GFP-VSR2 and RFP-VSR2 are strongly colocalized with a predominant population of yellow structures. Bars = 10 μm.

further insight into this process, we carefully evaluated the punctate distribution of the recycling-deficient mutant GFP-VSR2(L615A) with known organelle markers. Similar to the Y612A mutant, the L615A mutant is not retained in the Golgi apparatus (Figure 7A). However, it does not colocalize with markers for the TGN or the wild-type RFP-VSR2 fusion either (Figures 7B and 7C). In all cases, fluorescent signals clearly fell into two categories, either red or green, with only partial overlap seen for the combination GFP-VSR2(L615A) and wild-type RFP-VSR2 (Figure 7C). In conclusion, the L615A mutant does not show strong colocalization to any of the three organelle markers, in strong contrast with the wild-type fusion, which shows highest steady state levels in the PVC (Figure 4C), and the Y612A mutant, which accumulates mainly in the TGN (Figure 5B).

Although it is generally accepted that retromer-mediated retrieval of VSRs prevents exposure of receptors to the lytic environment of mammalian lysosomes, or yeast and plant vacuoles (Seaman, 2005; Bonifacino and Rojas, 2006; Oliviusson et al., 2006; Shimada et al., 2006; Jaillais et al., 2007; Yamazaki et al., 2008), it is not clear how vacuolar cargo reaches the vacuole. Is there an as yet uncharacterized vesicle carrier that delivers cargo from the PVC to the vacuole but excludes receptors, or does the PVC gradually mature by selective receptor retrieval alone? The latter case would predict the formation of a compartment with a different composition, enriched in cargo, that acquires fusion competence with the central vacuole when receptors have been depleted.

This hypothesis was tested with the soluble vacuolar marker Aleu-RFP, which was shown to label small fluorescent punctate structures at the cell periphery in addition to central vacuolar fluorescence (Figure 2A), both of which are replaced by apoplastic fluorescence when the functional competitor GFP-VSR2 (wt) is coexpressed (Figure 2B). However, the two point mutations strongly diminish in vivo competition, allowing Aleu-RFP to proceed normally to punctate structures and the vacuolar lumen. Coexpression of Aleu-RFP with GFP-VSR2(L615A) revealed a considerable correlation of Aleu-RFP fluorescence with GFP-VSR2(L615A) fluorescence, as seen by yellow signals in the merged image (Figure 7D). Correlation analysis revealed a typical diagonal pattern only in the scatterplot of Figure 7D. When coexpressed with markers for the Golgi apparatus or the TGN, Aleu-RFP forms clearly distinct punctae, giving rise to the typical segregation of two populations in the correlation analysis (see Supplemental Figures 1A and 1B online). As expected, also the TGN-retained GFP-VSR2(Y612A) mutant failed to colocalize with Aleu-RFP (see Supplemental Figure 1C online).

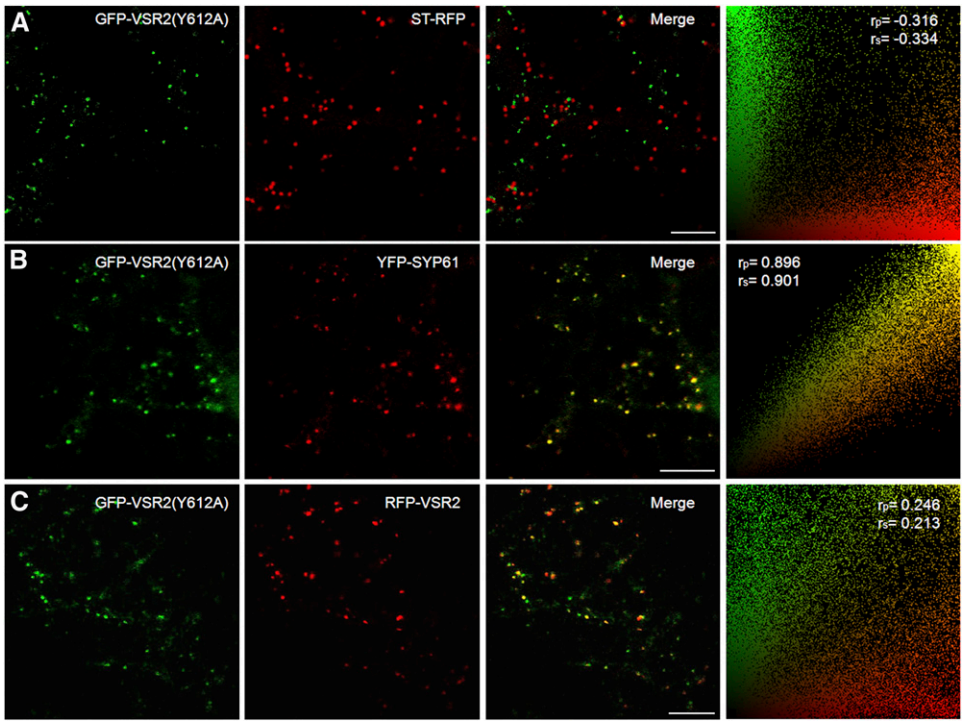

Figure 5. Quantitative Colocalization Analysis for GFP-VSR2(Y612A) with Known Organelle Markers.

In situ colocalization in tobacco leaf epidermis cells as in Figure 4, except that GFP-VSR2(Y612A) was used as test object coexpressed with either the Golgi marker ST-RFP **(A)**, the TGN marker YFP-SYP61 **(B)**, or the PVC marker RFP-VSR2 **(C)**. As in Figure 4, scatterplots at the right-hand side and associated Pearson or Spearman *r* values were obtained from a minimum of 400 individual punctae from at least 20 independent cell images. Notice that the mutant is no longer correlated with RFP-VSR2, but by far the strongest correlation was now found with the TGN marker YFP-SYP61. Bars = 10 μm.

Since the L615A mutant does not colocalize with markers for the Golgi or the TGN (Figures 7A and 7B), and there is considerable segregation into distinct structures between the wild-type VSR2 fusion and the L615A mutant (Figure 7C), the positive correlation between cargo and the mutant receptor indicates that the PVC may not be the last compartment before the vacuole in plants. The data are consistent with the presence of a different compartment that is positioned downstream of the PVC in the vacuolar transport pathway. This new compartment is enriched in soluble cargo, and in contrast with wild-type GFP-VSR2, the L615A mutant progresses to this compartment before it reaches the vacuole. We propose the term late PVC (LPVC) for this previously undiscovered compartment.

Attempts to generate stable transformants expressing full-length untagged VSR2(L615A) all led to undetectable expression of the VSR2 construct, in contrast with the wild-type receptor and its Y612A mutant (daSilva et al., 2006). This prevents us from carrying out ultrastructural studies but is again consistent with a generally higher turnover (Figure 3).

The Y612A Mutation Is Dominant over the L615A Mutation

So far, the obtained results suggest that the two mutations in the YMPL motif lead to opposite transport defects. The next question was to test how the receptor fusion is targeted when both mutations are superimposed on each other. We thus generated a GFP-VSR2 double mutant carrying both Y612A and L615A mutations (YMPL to AMPA) for coexpression with markers in the tobacco leaf epidermis system. Coexpression with the vacuolar cargo Aleu-RFP revealed a normal central vacuole stain (Figure 8A), indicative of impaired in vivo competition by GFP-VSR2 (AMPA). The mutant showed a fluorescence pattern similar to that of the single mutant GFP-VSR2(Y612A) in previous experiments (Figure 2C; see Supplemental Figure 1C online), labeling the plasma membrane as well as punctate structures, which were clearly distinct from Aleu-RFP punctae (Figure 8B). Further coexpression experiments with the TGN marker YFP-SYP61 and the single mutant GFP-VSR2(Y612A) and subsequent correlation analysis revealed a strong colocalization at the level of the TGN (Figures 8C and 8D).

Together, the results show that the anterograde transport defect caused by the Y612A mutation is dominant over the recycling defect imposed by the L615A mutation.

The Rab5 GTPase Rha1(RabF2a) Is Specifically Enriched at the LPVC

To rule out that LPVC structures are formed as a result of expression of an aberrant receptor, it was important to identify an independent marker for this putative organelle. For this reason, we

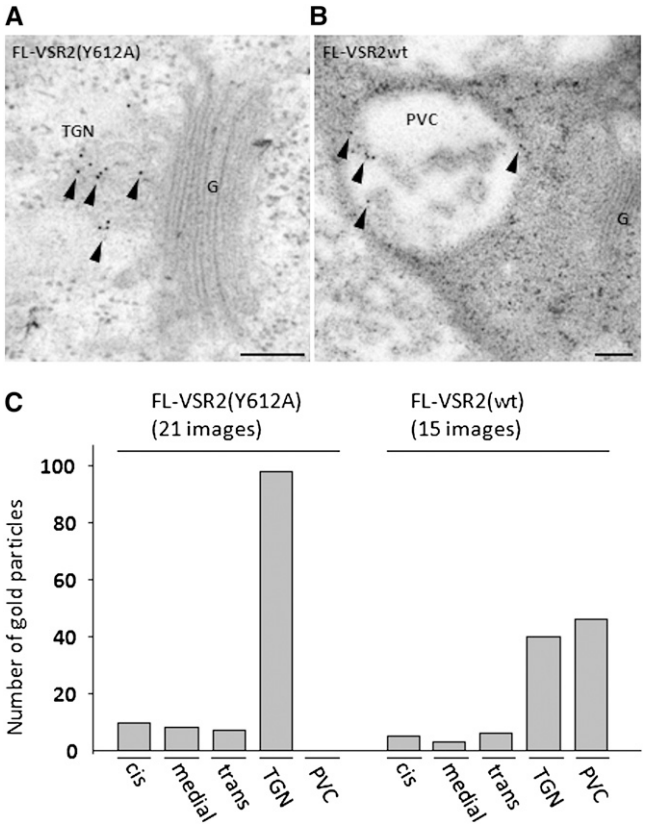

Figure 6. Ultrastructural Localization of Full-Length VSR2(wt) and VSR2 (Y612A).

(A) Electron micrograph showing immunogold-labeled FL-VSR2(Y612A) in root tip cells of transgenic tobacco plants (line described in da Silva et al., 2006).

(B) FL-VSR2(wt) is found in the PVC. Arrowheads indicate gold particles. Bars = 0.2 μm. wt, wild type.

(C) Numerical analysis of the distribution of gold particles over Golgi (*cis*, medial, or *trans*), TGN, and PVC.

considered known markers that were previously shown to label punctate organelles distinct from the Golgi bodies or the TGN. Members of the plant rab5 GTPase gene family have previously been shown to label PVC structures (Ueda et al., 2001, 2004; Sohn et al., 2003; Bolte et al., 2004; Kotzer et al., 2004; Lee et al., 2004). A systematic ultrastructural localization of the plant Rab5 GTPases Rha1 (RabF2a), Ara7 (RabF2b), and Ara6 (RabF1) revealed that they all label multivesicular bodies (Haas et al., 2007) and would thus be an excellent tool to localize them with respect to the suggested subdivision into PVC and LPVC. For this reason, we constructed a chimeric gene encoding a Venus-Rha1 fusion protein controlled by the weak mannopine synthase (TR2') promoter (Denecke et al., 1990) and performed quantitative correlation analysis with markers for the PVC and the putative LPVC.

Figure 9A illustrates that Venus-Rha1 and the PVC marker RFP-VSR2 appear to label two distinct populations of punctate structures. The scatterplot reveals two distinct populations but shows that the majority of green punctae also contain low levels of RFP-VSR2. This is demonstrated by a shift of the green population away from the *x* axis toward the diagonal. Punctate structures containing only red signals from RFP-VSR2 form a population close to the *y* axis. By contrast, coexpression of the GTPase fusion with the soluble vacuolar cargo Aleu-RFP shows predominantly a single population in the scatterplot, and PSC correlation values indicate strong colocalization (Figure 9B), even though minor segregation to mostly red or green can be observed at the boundaries of the population near the *x* and *y* axes.

The recycling-deficient L615A mutant of RFP-VSR2 shows an intermediate phenotype (Figure 9C), consistent with a partial colocalization between wild-type VSR2 and the L615A mutant (Figure 7C). Importantly, RFP-VSR2(L615A) exhibits a much stronger correlation with Venus-Rha1 compared with wild-type RFP-VSR2 (Figure 9A). The scatterplot shows a diagonal yellow population, even though a small number of structures labeled in red remain evident near the *y* axis.

Since neither VSR2 nor the soluble vacuolar cargo shows any colocalization with the Golgi and TGN bodies (Figures 4A and 4B; see Supplemental Figures 1A and 1B online), the results in Figure 9 provide evidence that the new LPVC structure does exist even when the L615A receptor mutant is not expressed. The work also illustrates that without quantitative PSC correlation analysis based on a large number of images, these shifts in steady state levels would have been very difficult to monitor. The scatterplots reveal interesting complexities, such as a minor proportion of RFP-VSR2 leaking to the LPVC (Figure 9A), or a minor proportion of RFP-VSR(L615A) in transit through the PVC (Figure 9C). The correlation values also show that the L615A mutant is shifted toward the LPVC and behaves more like soluble vacuolar cargo.

DISCUSSION

A Dual Role of YXXΦ in Anterograde and Retrograde VSR Transport

Many transport events in the secretory pathway depend on the continuous recycling of membranes and transport machinery. An important clue to the VSR recycling mechanism arose from the fact that the Y and Φ mutations within the same conserved canonical YXXΦ motif lead to opposite effects on VSR2 sorting. Figure 10A shows a summary of the Pearson and Spearman *r* values obtained for the two mutations when coexpressed with markers for the Golgi apparatus, the TGN, the PVC, and vacuolar cargo. Both VSR mutants show weak residual overlap with the wild-type VSR, which is not unexpected as neither mutation abolishes in vivo competition completely (Figure 1A). However, the results clearly illustrate a shift toward earlier or later compartments in the biosynthetic route to the vacuole. The Y mutation leads to an anterograde transport defect and retention in the TGN, an early compartment in the vacuolar route. By contrast, the Φ mutation interferes with retrograde transport and leads to increased leakage of VSRs together with its cargo to the LPVC. Increased vacuolar leakage of the Φ mutation was also shown biochemically (Figure 3A) and by microscopy (Figure 3B).

Figure 10B describes a transport model that can explain the observed results. Despite their opposite effect on VSR sorting,

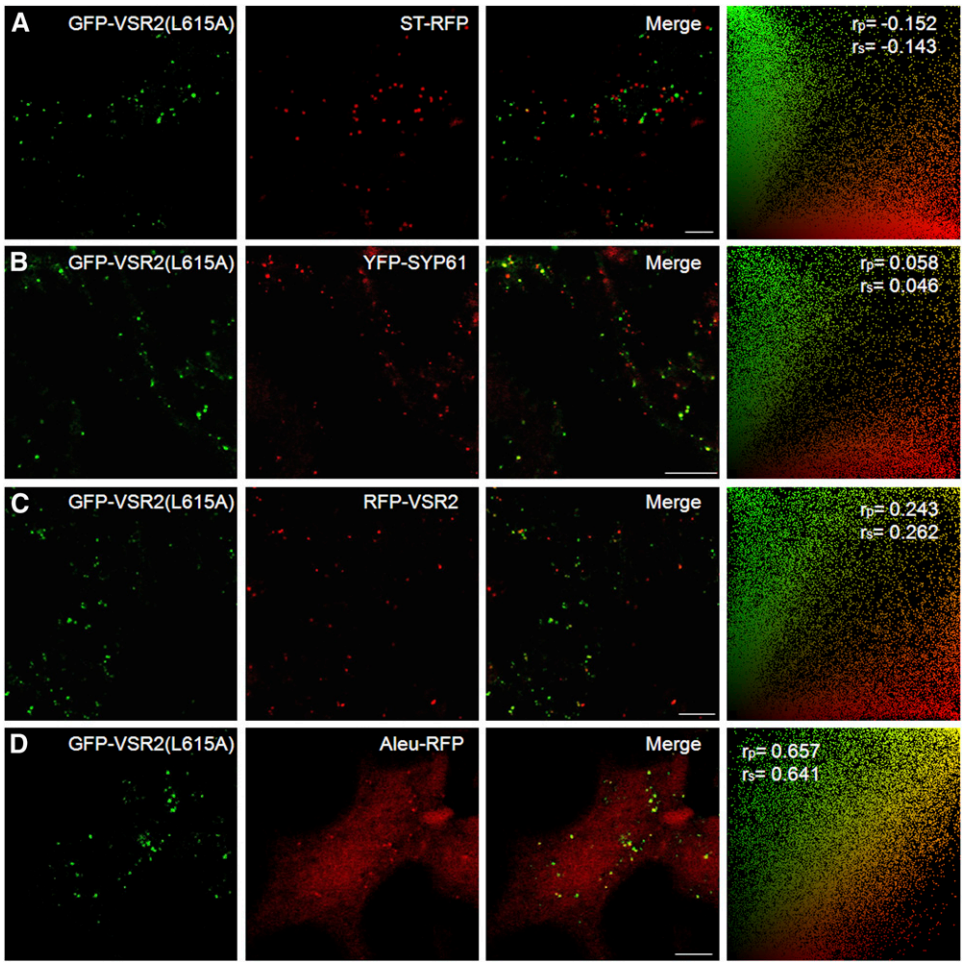

Figure 7. Correlation Colocalization Analysis for GFP-VSR2(L615A) with Known Organelle Markers.

In situ colocalization in tobacco leaf epidermis cells with GFP-VSR2(L615A) as test object. Coexpressions were performed with the Golgi marker ST-RFP **(A)**, the TGN marker YFP-SYP61 **(B)**, the PVC marker RFP-VSR2 **(C)**, or the soluble vacuolar cargo Aleu-RFP **(D)**. Notice that the strongest correlation was found with the soluble vacuolar marker Aleu-RFP. Bars = 10 μm.

the two mutations yielded a similar reduction for the in vivo competition assay (Figure 1A). The Φ mutant can reach the PVC but has lost the ability to recycle; hence, it will not compete with endogenous receptors and proceed to the LPVC and the vacuole. The Y mutation restricts progress toward the PVC and reduces the number of functional competitors at the level of the PVC. This explains why the competition assay provides the same readout for the two mutations (Figure 1A).

The fundamental difference between the two mutations becomes apparent in the reconstitution assay (Figure 1C). Since in vivo competition leads to saturation of the recycling route and increased turnover of endogenous VSRs (daSilva et al., 2005, 2006), overexpression of full-length VSRs continuously replenishes the pathway with functional receptors. These bind to cargo in the Golgi and deliver them to the PVC, even though recycling is saturated. Under these conditions, the ability to recycle is not important, and for this reason, the recycling-defective full-length VSR is able to reconstitute vacuolar sorting as well as the wild-type VSR (Figure 1C, gray bars). By contrast, the Y mutant of the full-length VSR binds to ligands and carries them to the cell surface where a low pH causes ligand release (daSilva et al., 2006). For this reason, it aggravates the effect of the competitor (Figure 1C, black bars). This effect is dominant and can cause induced secretion of vacuolar cargo when expressed on its own (Figure 2E, middle panel). The recycling-defective Φ mutant of the full-length VSR does not cause such effect (Figure 2E, right panel). This is also consistent with the model because this mutant would simply carry cargo to the PVC and then proceed further to the vacuole without causing harm.

The results suggest that plant VSRs employ a bipartite YxxΦ motif to control both anterograde as well as retrograde receptor transport. The sequential nature of these two events is illustrated by the double mutant in which both Y and Φ have been mutated and which behaves essentially like the single Y612A mutant (Figure 8).

It has been shown that both the Y and Φ residues associate with hydrophobic pockets in the μ2 subunit of AP2 adaptors in

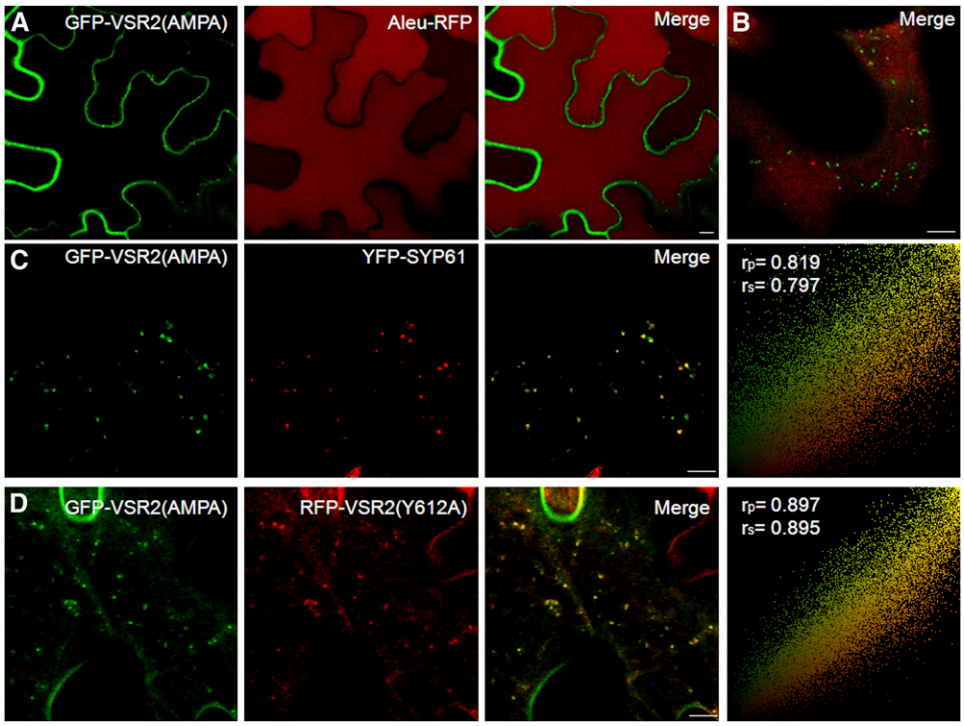

Figure 8. Dominance of the Anterograde Transport Defect (Y612A) over the Retrograde Transport Defect (L615A).

(A) In situ coexpression experiment in tobacco leaf epidermis cells with the double (Y612A + L615A) mutant GFP-VSR2(AMPA) with vacuolar cargo Aleu-RFP, showing normal vacuolar RFP fluorescence and peripheral+punctate green fluorescence for the VSR2 fusion.
(B) A portion of a cell from **(A)** but imaged at higher magnification and at the cell cortex to illustrate noncolocalization of punctate structures.
(C) In situ colocalization of GFP-VSR2(AMPA) with the TGN-marker YFP-SYP61. Notice a strong correlation with the TGN marker.
(D) As in **(C)** but GFP-VSR2(AMPA) was coexpressed with the single mutant RFP-VSR2(Y612A). The strong correlation indicates dominance of Y612A over the L615A mutation.
Bars = 5 μm in all panels.

vitro (Ohno et al., 1995; Owen and Evans, 1998), but this does not exclude the possibility that the Y and Φ positions are in fact part of two distinct but overlapping sorting motifs. Indeed, efficient recycling would require that the tail can interface with different cytosolic transport machineries dependent on which organelle it resides, and overlapping sorting structures would render the different recruitment activities mutually exclusive.

The exact lipid composition and other membrane residents in the donor and receptor compartments may stimulate the specific exposure of one but not the other sorting signal, possibly further fine-tuned by specific modifications of the tail. In this respect, it is interesting to note that the phosphorylation status of YXXΦ can modulate interaction with clathrin adaptors (Shiratori et al., 1997). It will also be interesting to test the mutation of the hydrophobic residue in YxxΦ motifs of other proteins, including those of nonplant cell systems, to verify with in vivo trafficking assays if bipartite YxxΦs are a plant-specific feature or more generally applicable.

The Role of YXXΦ in Selective Anterograde VSR Transport

We have previously shown that the Y mutation causes partial VSR mistargeting to the plasma membrane and another compartment that was neither Golgi nor PVC (daSilva et al., 2006). Here, we provided conclusive evidence to show that this compartment is the TGN (Figures 5 and 6). High steady state levels of the Y mutant in the TGN can be explained by various refinements of our model (Figure 10B).

The vectorial transport model (Palade, 1975) would predict that plant VSRs migrate from the endoplasmic reticulum (ER) via the Golgi apparatus to the TGN. The latter is coated with clathrin in plants (Staehelin and Moore, 1995), strongly suggesting that cargo-loaded VSRs exit the TGN in CCVs to reach the PVC. If the Y mutation prevents VSR-mediated recruitment of clathrin adaptors (Happel et al., 2004), the Y mutant of the receptor would accumulate in the TGN until bulk flow could lead to overflow to the plasma membrane. This model would place the TGN as the main sorting station to segregate secretory from vacuolar cargo and supports the recent proposition that TGNs mature by selective retrieval of vacuolar cargo to form secretory vesicle clusters (Toyooka et al., 2009).

However, it is equally possible that VSRs normally bypass the TGN and leave the Golgi stack directly (Hillmer et al., 2001). If the Y mutation prevents Golgi-mediated CCV budding, the mutant receptor may simply progress and accumulate in the TGN as the next organelle in the pathway. But since the plant TGN has been

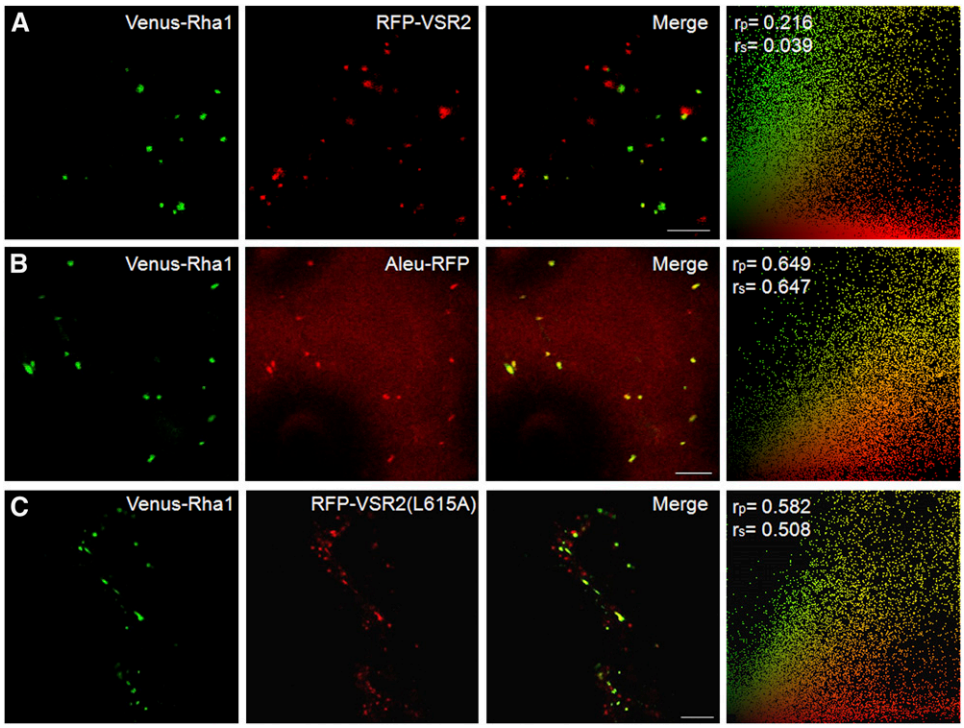

Figure 9. The Rab5 GTPase Rha1(RabF2a) Is a Marker for the LPVC.

In situ coexpression experiment in tobacco leaf epidermis cells using Venus-Rha1 (green) as test object. Coexpressions were performed with either wild-type RFP-VSR2 as a PVC marker **(A)**, the soluble vacuolar cargo Aleu-RFP as a LPVC marker **(B)**, and the recycling defective RFP-VSR2(L615A) as a putative LPVC marker **(C)**, all of which are shown in red. Notice that both Aleu-RFP and RFP-VSR2(L615A) show much higher correlation coefficients when coexpressed with Venus-Rha1 compared with the wild-type RFP-VSR2. Bars = 10 μm.

shown to act as the first organelle in the endocytic route (Dettmer et al., 2006; Lam et al., 2007a, 2007b) we cannot rule out that the Y mutant of the receptor first moves to the plasma membrane and then undergoes nonclathrin-mediated endocytosis to reach the TGN, where it would accumulate since it cannot exit in CCVs to proceed to the PVC. Currently, all these scenarios have to be considered until experimental evidence is provided in living cells showing that TGN-resident markers are first detected at the Golgi stack immediately prior to their detection at the TGN. Although technically demanding due to organelle motion, photoactivatable GFP fusions may be the key to answering this fundamental question about the role of the TGN in biosynthetic transport to the vacuoles and the plasma membrane.

While plant retromer components have been consistently localized to the PVC (Oliviusson et al., 2006; Shimada et al., 2006; Jaillais et al., 2007; Phan et al., 2008; Yamazaki et al., 2008), it has recently been reported that some retromer components may localize to the TGN instead (Niemes et al., 2010). The authors suggested that retromer-mediated receptor retrieval occurs from the TGN rather than the PVC and that released vacuolar cargo proceeds further by unspecific bulk flow, although it is unclear how secretory and vacuolar cargo would then be effectively segregated.

Results presented here strongly argue against this idea because arrival of VSR2 at the PVC is clearly signal dependent and sensitive to the Y mutation. Furthermore, also the recycling of VSR from the PVC is signal dependent as demonstrated by the Φ mutation (Figure 7), consistent with the PVC as site for VSR retrieval. By analogy to the GTPase ARF1, which is clearly involved in multiple transport processes in the plant secretory pathway (Geldner et al., 2003; Pimpl et al., 2003), it is possible that retromer-mediated transport processes are not restricted to the retrieval of plant VSRs from the PVC but may also play a role in endocytic recycling (Jaillais et al., 2006, 2007, 2008) and that both pathways influence each other. In the light of our results, it will be interesting in the future to reevaluate the subcellular localization of all known retromer components and to test the influence of retromer mutants using experiments that involve both biosynthetic and endocytic cargo molecules.

Interesting parallels can also be drawn from observations with the drug wortmannin, which was shown to inhibit VSR recycling (daSilva et al., 2005), leading to colocalization of TGN and PVC markers in enlarged vacuolated structures (Wang et al., 2009). If PVC-to-LPVC maturation depends on the selective retrieval of VSRs, then it stands to reason that wortmannin would cause a maturation defect, but it is remarkable that it also leads to fusion with the TGN. Precedence for such scenario in the early secretory pathway arose two decades ago from observations with the drug Brefeldin A, which causes fusion of entire Golgi cisternae with the ER (Lippincott-Schwartz et al., 1989). It was later shown

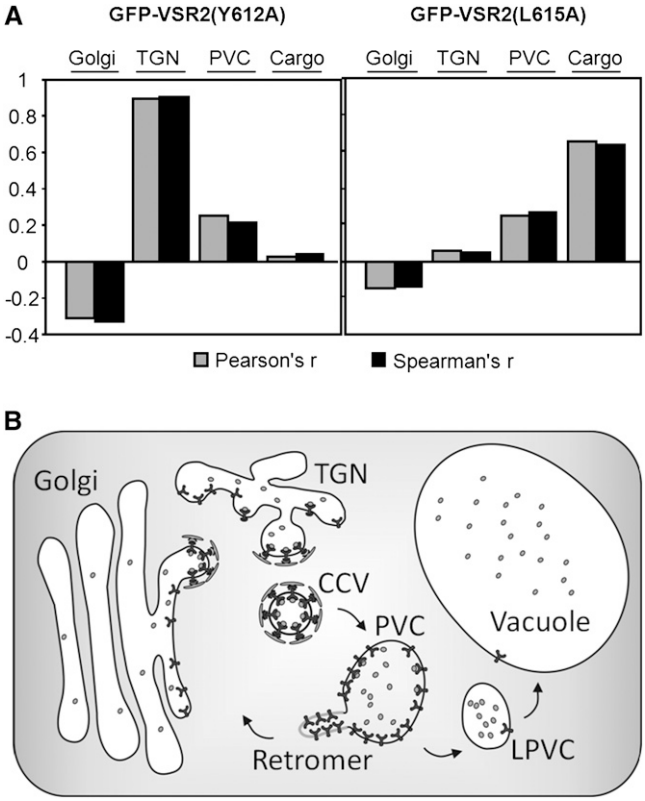

Figure 10. Working Model for VSR Traffic and PVC Maturation.

(A) Summary of Pearson (gray) and Spearman (black) *r* values illustrating the opposite polarity of the two trafficking mutants, Y612A and L615A. While the Y612A mutant shows the highest steady state levels in the TGN, the L615A mutant is colocalized mainly with the vacuolar cargo, and both mutants show only partial colocalization with the PVC resident wild-type VSR2 fusion protein.

(B) Illustration of the model: CCVs may bud from either the Golgi cisternae or the TGN and carry VSR-ligand complexes to the PVC where ligands dissociate. Unoccupied receptors recruit retromer and are selectively retrieved. This may lead to maturation of an LPVC, which contains mainly cargo, no longer accepts incoming CCVs, and has acquired competence for fusion with the vacuolar membrane. Under normal physiological conditions, only minor quantities of VSRs reach the LPVC and the vacuole because they recycle back to the early secretory pathway. The exact acceptor compartment for the recycling route remains to be identified.

that the primary effect of the drug causes titration of the GTPase ARF1 in an abortive complex with its exchange factor, leading to inhibition of retrograde COPI-mediated Golgi-to-ER transport (Peyroche et al., 1999). The selective retrieval of key components to regulate organelle maturation may thus be a conserved principle at various levels of the secretory pathway.

Evidence for an LPVC in Plants

Localization analyses of the VSR fusions and vacuolar cargo provide compelling evidence for the existence of a new compartment, the LPVC. Both the Y mutant and the Φ mutant segregate from the PVC-resident wild-type receptor, but only the Φ mutant colocalizes with cargo in punctate structures (Figures 7 and 10A) and the vacuolar lumen (Figure 3). This suggests that the cargo-containing LPVC is situated between the PVC and the vacuole. These results are strongly supported by the fact that Rab5 GTPase Rha1 is an independent marker for the LPVC (Figure 9), showing that LPVC structures are not an artifact caused by expression of an aberrant receptor molecule.

Earlier efforts on the localization of VSRs and their cargo provide support for our current working hypothesis. Using an mRFPAtVSR2 fusion and the lytic vacuole marker aleurain-GFP, it was shown that colocalization of the two markers is not absolute, and structures highlighted by aleurain-GFP but not mRFPAtVSR2 may well have represented LPVCs (Miao et al., 2008).

The inclusion of the Rab5 GTPase as an independent LPVC marker (Figure 9) permitted us to refine earlier results on the localization of this class of GTPase (Ueda et al., 2001, 2004; Sohn et al., 2003; Bolte et al., 2004; Kotzer et al., 2004; Lee et al., 2004; Haas et al., 2007). In addition, we can speculate about the nature of the LPVC because it has been shown that the three *Arabidopsis* rab5 GTPases are found to localize to multivesicular bodies using immunogold electron microscopy (Haas et al., 2007). For this reason, it is very likely that both PVC and LPVC exhibit a multivesicular morphology. Internal vesicles are destined for vacuolar degradation and should not be affected by the process of receptor retrieval from the delimiting membrane. The differences between PVC and LPVC are thus likely to be restricted to the exact lipid and protein composition of the delimiting membrane.

The simplest explanation for the obtained results is a transport model in which PVCs gradually mature into LPVCs by selective signal-mediated receptor retrieval (Figure 10B). Wild-type receptors would normally be excluded from the LPVC, although a minor rate of vacuolar VSR turnover would permit renewal of the receptor population and replace damaged, nonfunctional VSRs. Since the Φ mutant is recycling defective, it behaves more like the vacuolar cargo itself and segregates together to the LPVC en route to the vacuole.

In addition to the organelle maturation model, more complex scenarios can be envisaged that involve vesicle shuttles between the PVC and the LPVC. However, in the absence of evidence for such vesicles, the maturation model represents the simplest solution to explain existing data and leads to two important predictions that can be made about the nature of the LPVC. After reaching a critical mass of VSRs in the PVC membranes and subsequent ligand release, fusion competence with newly arriving CCVs should be inhibited. This is essential to permit efficient receptor depletion by selective retrieval. Likewise, receptor depletion in the LPVC should be accompanied by an acquired competence for fusion with the vacuolar membrane. This could be achieved by a different composition of tethering factors and SNAREs displayed on the LPVC surface compared with that of the PVC.

The tools generated in this work open up the prospect of enriching LPVCs from PVCs by small particle flow cytometry and/or affinity-aided organelle sorting. Comparative proteomics of PVC and LPVC populations may lead to the identification

of new membrane residents or membrane-associated proteins, allowing us to test the predictions of our model and shed light on the fundamental molecular mechanisms that allow cargo but not receptors to reach the vacuole.

METHODS

Recombinant DNA Constructs

All DNA manipulations were performed according to established procedures. The highly competent *Escherichia coli* MC1061 strain (Casadaban and Cohen, 1980) was used for the routine amplification of all plasmids. Previously established plasmids were used, including Amy-spo (Pimpl et al., 2003; daSilva et al., 2005), GFP-HDEL (Brandizzi et al., 2003), GFP-VSR2 (GFP-BP80) (daSilva et al., 2005), GFP-VSR2(Y612A), GFP-VSR2 (L615A) (daSilva et al., 2006), full-length VSR2, and full-length VSR2 (Y612A) (daSilva et al., 2006).

To produce the L615A mutation on the full-length VSR2, the QuickChange method (Stratagene) was used with pairs of oligonucleotides encoding for the mutated triplet and 15 bases extending on either side of the mutated codon (L615A-labeled oligonucleotide sequences are shown in Supplemental Table 1 online).

To generate the YFP-SYP61 fusion, the full-length coding region of SYP61 was amplified using oligonucleotides described in Supplemental Table 1 online, from first-strand cDNA from 5-d-old seedlings prepared as described previously (Pimpl et al., 2003). This results in the engineering of restriction site *Cla*I overlapping with the N-terminal start codon (Met) and the restriction site *Xba*I just following the stop codon of the SYP61 coding region. The obtained PCR fragment was digested with *Cla*I and *Xba*I, gel purified, and ligated into pOF21 (Foresti et al., 2006) that was cut with *Cla*I and *Xba*I, followed by dephosphorylation, to replace the SYP21 coding region by that of SYP61. This yielded plasmid pOF61 (YFP-SYP61).

ST-RFP was created by amplification of the ST sequence from ST-YFP (daSilva et al., 2005) using oligonucleotides described in Supplemental Table 1 online to introduce *Cla*I and *Sal*I restriction sites at the N terminus and C terminus of the coding sequence, respectively. The RFP coding sequence was amplified using oligonucleotides to introduce *Sal*I and *Bam*HI restriction sites at the N terminus and C terminus, respectively. The two fragments were digested with the appropriate restriction enzyme and inserted in frame through a two-fragment ligation in a vector derived from pOF19 (Foresti et al., 2006) by digestion with *Cla*I and *Bam*HI followed by dephosphorylation. This yielded plasmid pOF53 (ST-RFP).

Aleu-RFP was created by amplification of the Aleurain propeptide sequence from Aleu-GFP (Di Sansebastiano et al., 2001) using oligonucleotides described in Supplemental Table 1 online to introduce *Cla*I and *Nhe*I restriction sites at the N terminus and C terminus of the coding sequence, respectively. The RFP coding sequence was amplified using oligonucleotides to introduce *Nhe*I and *Bam*HI restriction sites at the N terminus and C terminus, respectively. The two fragments were digested with the appropriate restriction enzyme and inserted in frame through a two-fragment ligation in a vector obtained from pOF19 (Foresti et al., 2006) digested with *Cla*I and *Bam*HI. This yielded plasmid pAW7 (Aleu-RFP).

To generate an RFP-VSR2 fusion, we replaced the YFP portion of YFP-BP80 (VSR2) (daSilva et al., 2006) with RFP. We thus amplified RFP using oligonucleotides described in Supplemental Table 1 online to introduce *Nhe*I and *Bgl*II restriction sites at the N terminus and C terminus, respectively. The PCR fragment was digested with *Nhe*I and *Bgl*II to yield a fragment that replaced the equivalent portion in YFP-BP80. This yielded plasmid pOF100 encoding RFP-VSR2 that carries a signal peptide of sweet potato (*Ipomoea batatas*) sporamin for insertion into the ER, followed by RFP and the transmembrane domain and cytosolic tail of VSR2.

To generate the Venus-Rha1 fusion, coding regions for Venus and Rha1 were amplified with primers shown in Supplemental Table 1 online to introduce *Cla*I and *Nco*I flanking Venus and *Nco*I-*Xba*I flanking Rha1, for insertion into pOF19 (Foresti et al., 2006) cut with *Cla*I and *Xba*I, yielding plasmid pFB28. The TR2' promoter fragment was amplified from pOP443 (Velten et al., 1984) using the primers shown in Supplemental Table 1 online to generate an *Eco*RI-*Cla*I fragment. The Venus-Rha1 coding region, together with 3′nos, was cut from pFB28 as a *Cla*I-*Hin*dIII fragment and inserted together with the *Eco*RI-*Cla*I TR2' promoter fragment into the polylinker of pGSC1700 (Cornelissen and Vandewiele, 1989) to yield pTDCG9.

All DNA coding sequences of the fluorescent chimeric genes, flanked by the cauliflower mosaic virus 35S promoter and the 3′-untranslated end of the nopaline synthase gene (3′nos), were finally inserted as an *Eco*RI-*Hin*dIII fragment into the polylinker of the *Agrobacterium tumefaciens* transformation vector pDE1001 (Denecke et al., 1992).

All plant transformation plasmids were transfected into the *Agrobacterium* rifampicin-resistant strain C58C1Rif^R (pGV2260) as described previously (Denecke et al., 1992).

Plant Material and Transient Protoplast Expression Procedure

Plants of *Nicotiana tabacum* cv Petit Havana (Maliga et al., 1973) were grown from surface-sterilized seeds in Murashige and Skoog medium (Murashige and Skoog, 1962) and 2% sucrose in a controlled room at 22°C with a 16-h daylength at a light irradiance of 200 mE/m^2/s. Leaf protoplasts were obtained after overnight digestion in TEX buffer (B5 salts, 500 mg/L MES, 750 mg/L $CaCl_2[2H_2O]$, 250 mg/L NH_4NO_3, and 0.4M sucrose, pH 5.7) with 0.2% Macerozyme R10 and 0.4% Cellulase R10 (Yakult) and washed in electroporation buffer (2.4 g/L HEPES, 6 g/L KCl, 600 mg/L $CaCl_2$, and 0.4M sucrose, pH 7.2). Protoplast aliquots (500 μL) were transfected by electroporation at a density of 5×10^6 protoplasts/mL using a stainless steel electrode at a distance of 3.5 mm and a complete exponential discharge of a 1000-μF capacitor charged at 160 V. After 15 min, electroporated protoplast samples were diluted with 2 mL of TEX buffer, followed by 24-h incubation at 22°C in darkness. Harvesting of clear cell-free medium was done manually using a refined Pasteur pipette from underneath the layer of floating protoplasts obtained after 5 min of centrifugation at 100*g* in a swing-out rotor. The total cell population of the cell suspension was obtained by washing the cells in a 10-fold excess of 250 mM NaCl, centrifugation at 200*g* for 3 min, and recovery of the thus washed cell pellet on ice. A detailed description of the entire protocol was published previously (Foresti et al., 2006).

α-Amylase Assay and Secretion Index Determinations

Preparation of cell and medium fractions and determination of extracellular (secreted) and intracellular α-amylase activities were performed as described before (daSilva et al., 2006). The secretion index is defined as the ratio of extracellular to intracellular reporter activities (Denecke et al., 1990).

Protein Extraction and Gel Blot Analysis

Protoplasts from 2.5-mL suspensions were pelleted with 250 mM NaCl and resuspended in 250 mL of leaf extraction buffer (100 mM Tris-HCl, pH 7.8, 200 mM NaCl, 1 mM EDTA, 0.2% Triton X-100, and 2% β-mercaptoethanol), followed by brief sonication and 10-min centrifugation at 25,000*g* at 48°C. Infiltrated leaf sections were extracted directly in leaf extraction buffer with pestle and mortar. The supernatant containing both soluble and membrane proteins was recovered and subsequently used for protein gel blotting analysis as previously described (Pimpl et al., 2006). For immunodetection, we used rabbit polyclonal antiserum raised against either VSR2 (1:5000 dilution) (Tse et al., 2004) or GFP (1:5000 dilution; Molecular Probes).

Tobacco Leaf Infiltration Procedure

Soil-grown *N. tabacum* cv Petit Havana (Maliga et al., 1973) was infiltrated with *Agrobacterium* cultures (at OD 0.1) as described previously (Sparkes et al., 2006) and analyzed after 2 d of further growth by confocal laser scanning microscopy.

Fluorescence Confocal Microscope Imaging and Analysis

Infiltrated tobacco leaf squares (0.5 × 0.5 cm) were mounted in tap water with the lower epidermis facing the thin cover glass (22 × 50 mm; No. 0). Confocal imaging was performed using an upright Zeiss LSM 510 META laser scanning microscope (Zeiss) with a Plan-Neofluar ×40/1.3 oil differential interference contrast objective. For imaging of the coexpression of YFP and GFP constructs, excitation lines of an argon ion laser of 458 nm for GFP and 514 nm for YFP were used alternately with line switching on the multitrack facility of the microscope. Fluorescence was detected using a 545-nm dichroic beam splitter and a 480- to 520-nm band-pass filter for GFP and a 565- to 615-nm band-pass filter for YFP. For imaging of the coexpression of GFP and RFP constructs, or Venus and RFP constructs, excitation lines of an argon ion laser of 488 nm for GFP/Venus and of a He/Ne 543 nm for RFP were used alternately with line switching on the multitrack facility of the microscope. Fluorescence was detected using a 545-nm dichroic beam splitter and a 500- to 530-nm narrow band-pass filter for GFP/Venus and a 565- to 615-nm band-pass filter for RFP. Postacquisition image processing was performed with the LSM 5 image browser (Zeiss) and ImageJ (Abramoff et al., 2004; see also http://rsb.info.gov/ij/).

Image analysis was undertaken using the LSM 5 image browser (Zeiss) for line scans and the ImageJ analysis program (Abramoff et al., 2004) and the PSC colocalization plug-in (French et al., 2008) to calculate colocalization and to produce scatterplots. Results are presented either as Pearson correlation coefficients, which represent the linear relationship of the signal intensity from the green and red channels of the analyzed image or as Spearman's rank correlation coefficients that take into account nonlinear relationships as well. Both tests produce values in the range [−1, 1], where 0 indicates no discernable correlation and −1 and +1 indicate strong negative or positive correlations, respectively. The program allowed masking of areas to be included in the analysis. In a given image, all punctate structures were masked prior to analysis using the selection brush tool as described (French et al., 2008). A threshold level of 10 was set, under which pixel values were considered noise and not included in the statistical analysis. At least 20 cells or at least 400 independent punctate structures were analyzed for each condition.

Electron Microscopy

Samples were high-pressure frozen using a Baltec HPF010 high-pressure freezer and freeze-substituted in the presence of 0.5% uranyl acetate in methanol using a Reichert AFS freeze-substitution apparatus (Leica), and the temperature was gradually increased from −160°C to −20°C. Samples were infiltrated with LR White resin from 10 to 100% at −20°C over several days and polymerized at −20°C with UV light. Sections (70 nm) were cut with a RMC PowerTome ultramicrotome (Boeckeler Instruments). For immunolabeling, sections were first blocked in 1% BSAc, 1% goat serum, and 0.1% fish gelatin in Tris-HCl buffer for 30 min,. followed by three washes with 0.1% BSAc. Labeling was with rabbit antibodies raised against the lumenal portion of VSR2 (Tse et al., 2004) 1:100 overnight followed by three washes with 0.1% BSAc in Tris-HCl buffer prior to incubation for 90 min in a 1:20 dilution of 10-nm gold conjugated goat anti-rabbit IgG (BB International). After three washes in 0.1% BSAc and three washes in water, sections were poststained for 15 min with 1% uranyl acetate and lead citrate.

Accession Number

The sequence of the *Arabidopsis thaliana* VSR isoform VSR2 studied in this article can be found in the Arabidopsis Genome Initiative or GenBank/EMBL databases under accession number AT2G14720.

Supplemental Data

The following materials are available in the online version of this article.

Supplemental Figure 1. Coexpression Analysis in Tobacco Leaf Epidermis Cells Testing the Soluble Vacuolar Cargo Aleu-RFP against the Golgi Marker ST-YFP, the TGN Marker YFP-SYP61, and the TGN-Retained Mutant GFP-VSR2(Y612A).

Supplemental Table 1. Primers Used in This Work.

ACKNOWLEDGMENTS

We thank Luis L.P. daSilva (University of São Paulo, Ribeirão Preto, Brazil) for scientific discussion and critically reading of this manuscript. We also thank Liwen Jiang (Chinese University of Hong Kong, China) for the most generous gift of two antisera, one of which raised against the cytosolic tail of VSR2 and one against the lumenal domain. This work was supported by the Biotechnology and Biological Sciences Research Council Project BB/D016223/1 and The Leverhulme Trust (F/10 105/E).

Received July 29, 2010; revised October 4, 2010; accepted November 11, 2010; published December 21, 2010.

REFERENCES

Abramoff, M.D., Magelhaes, P.J., and Ram, S.J. (2004). Image processing with ImageJ. Biophotonics International **11:** 36–42.

Bolte, S., Brown, S., and Satiat-Jeunemaitre, B. (2004). The N-myristoylated Rab-GTPase m-Rabmc is involved in post-Golgi trafficking events to the lytic vacuole in plant cells. J. Cell Sci. **117:** 943–954.

Bonifacino, J.S., and Dell'Angelica, E.C. (1999). Molecular bases for the recognition of tyrosine-based sorting signals. J. Cell Biol. **145:** 923–926.

Bonifacino, J.S., and Glick, B.S. (2004). The mechanisms of vesicle budding and fusion. Cell **116:** 153–166.

Bonifacino, J.S., and Rojas, R. (2006). Retrograde transport from endosomes to the trans-Golgi network. Nat. Rev. Mol. Cell Biol. **7:** 568–579.

Brandizzi, F., Hanton, S., DaSilva, L.L., Boevink, P., Evans, D., Oparka, K., Denecke, J., and Hawes, C. (2003). ER quality control can lead to retrograde transport from the ER lumen to the cytosol and the nucleoplasm in plants. Plant J. **34:** 269–281.

Casadaban, M.J., and Cohen, S.N. (1980). Analysis of gene control signals by DNA fusion and cloning in Escherichia coli. J. Mol. Biol. **138:** 179–207.

Cornelissen, M., and Vandewiele, M. (1989). Nuclear transcriptional activity of the tobacco plastid psbA promoter. Nucleic Acids Res. **17:** 19–29.

daSilva, L.L., Foresti, O., and Denecke, J. (2006). Targeting of the plant vacuolar sorting receptor BP80 is dependent on multiple sorting signals in the cytosolic tail. Plant Cell **18:** 1477–1497.

daSilva, L.L., Taylor, J.P., Hadlington, J.L., Hanton, S.L., Snowden, C.J., Fox, S.J., Foresti, O., Brandizzi, F., and Denecke, J. (2005). Receptor salvage from the prevacuolar compartment is essential for efficient vacuolar protein targeting. Plant Cell **17:** 132–148.

Denecke, J., Botterman, J., and Deblaere, R. (1990). Protein secretion in plant cells can occur via a default pathway. Plant Cell **2:** 51–59.

Denecke, J., De Rycke, R., and Botterman, J. (1992). Plant and mammalian sorting signals for protein retention in the endoplasmic reticulum contain a conserved epitope. EMBO J. **11:** 2345–2355.

Dettmer, J., Hong-Hermesdorf, A., Stierhof, Y.D., and Schumacher, K. (2006). Vacuolar H+-ATPase activity is required for endocytic and secretory trafficking in *Arabidopsis*. Plant Cell **18:** 715–730.

Di Sansebastiano, G.P., Paris, N., Marc-Martin, S., and Neuhaus, J.M. (2001). Regeneration of a lytic central vacuole and of neutral peripheral vacuoles can be visualized by green fluorescent proteins targeted to either type of vacuoles. Plant Physiol. **126:** 78–86.

Foresti, O., daSilva, L.L., and Denecke, J. (2006). Overexpression of the *Arabidopsis* syntaxin PEP12/SYP21 inhibits transport from the prevacuolar compartment to the lytic vacuole in vivo. Plant Cell **18:** 2275–2293.

Foresti, O., and Denecke, J. (2008). Intermediate organelles of the plant secretory pathway: Identity and function. Traffic **9:** 1599–1612.

French, A.P., Mills, S., Swarup, R., Bennett, M.J., and Pridmore, T.P. (2008). Colocalization of fluorescent markers in confocal microscope images of plant cells. Nat. Protoc. **3:** 619–628.

Geldner, N., Anders, N., Wolters, H., Keicher, J., Kornberger, W., Muller, P., Delbarre, A., Ueda, T., Nakano, A., and Jürgens, G. (2003). The Arabidopsis GNOM ARF-GEF mediates endosomal recycling, auxin transport, and auxin-dependent plant growth. Cell **112:** 219–230.

Haas, T.J., Sliwinski, M.K., Martínez, D.E., Preuss, M., Ebine, K., Ueda, T., Nielsen, E., Odorizzi, G., and Otegui, M.S. (2007). The *Arabidopsis* AAA ATPase SKD1 is involved in multivesicular endosome function and interacts with its positive regulator LYST-INTERACTING PROTEIN5. Plant Cell **19:** 1295–1312.

Happel, N., Höning, S., Neuhaus, J.M., Paris, N., Robinson, D.G., and Holstein, S.E. (2004). Arabidopsis mu A-adaptin interacts with the tyrosine motif of the vacuolar sorting receptor VSR-PS1. Plant J. **37:** 678–693.

Hillmer, S., Movafeghi, A., Robinson, D.G., and Hinz, G. (2001). Vacuolar storage proteins are sorted in the cis-cisternae of the pea cotyledon Golgi apparatus. J. Cell Biol. **152:** 41–50.

Höning, S., Griffith, J., Geuze, H.J., and Hunziker, W. (1996). The tyrosine-based lysosomal targeting signal in lamp-1 mediates sorting into Golgi-derived clathrin-coated vesicles. EMBO J. **15:** 5230–5239.

Hunter, P.R., Craddock, C.P., Di Benedetto, S., Roberts, L.M., and Frigerio, L. (2007). Fluorescent reporter proteins for the tonoplast and the vacuolar lumen identify a single vacuolar compartment in Arabidopsis cells. Plant Physiol. **145:** 1371–1382.

Jaillais, Y., Fobis-Loisy, I., Miège, C., and Gaude, T. (2008). Evidence for a sorting endosome in Arabidopsis root cells. Plant J. **53:** 237–247.

Jaillais, Y., Fobis-Loisy, I., Miège, C., Rollin, C., and Gaude, T. (2006). AtSNX1 defines an endosome for auxin-carrier trafficking in Arabidopsis. Nature **443:** 106–109.

Jaillais, Y., Santambrogio, M., Rozier, F., Fobis-Loisy, I., Miège, C., and Gaude, T. (2007). The retromer protein VPS29 links cell polarity and organ initiation in plants. Cell **130:** 1057–1070.

Jurgens, G. (2004). Membrane trafficking in plants. Annu. Rev. Cell Dev. Biol. **20:** 481–504.

Kirsch, T., Paris, N., Butler, J.M., Beevers, L., and Rogers, J.C. (1994). Purification and initial characterization of a potential plant vacuolar targeting receptor. Proc. Natl. Acad. Sci. USA **91:** 3403–3407.

Kirsch, T., Saalbach, G., Raikhel, N.V., and Beevers, L. (1996). Interaction of a potential vacuolar targeting receptor with amino- and carboxyl-terminal targeting determinants. Plant Physiol. **111:** 469–474.

Kotzer, A.M., Brandizzi, F., Neumann, U., Paris, N., Moore, I., and Hawes, C. (2004). AtRabF2b (Ara7) acts on the vacuolar trafficking pathway in tobacco leaf epidermal cells. J. Cell Sci. **117:** 6377–6389.

Lam, S.K., Siu, C.L., Hillmer, S., Jang, S., An, G., Robinson, D.G., and Jiang, L. (2007b). Rice SCAMP1 defines clathrin-coated, trans-golgi-located tubular-vesicular structures as an early endosome in tobacco BY-2 cells. Plant Cell **19:** 296–319.

Lam, S.K., Tse, Y.C., Robinson, D.G., and Jiang, L. (2007a). Tracking down the elusive early endosome. Trends Plant Sci. **12:** 497–505.

Lee, G.J., Sohn, E.J., Lee, M.H., and Hwang, I. (2004). The Arabidopsis rab5 homologs rha1 and ara7 localize to the prevacuolar compartment. Plant Cell Physiol. **45:** 1211–1220.

Lippincott-Schwartz, J., Yuan, L.C., Bonifacino, J.S., and Klausner, R.D. (1989). Rapid redistribution of Golgi proteins into the ER in cells treated with brefeldin A: Evidence for membrane cycling from Golgi to ER. Cell **56:** 801–813.

Maliga, P., Sz-Breznovits, A., and Márton, L. (1973). Streptomycin-resistant plants from callus culture of haploid tobacco. Nat. New Biol. **244:** 29–30.

Miao, Y., Li, K.Y., Li, H.Y., Yao, X., and Jiang, L. (2008). The vacuolar transport of aleurain-GFP and 2S albumin-GFP fusions is mediated by the same pre-vacuolar compartments in tobacco BY-2 and Arabidopsis suspension cultured cells. Plant J. **56:** 824–839.

Murashige, T., and Skoog, F. (1962). A revised medium for rapid growth and bio assays with tobacco tissue cultures. Physiol. Plant. **15:** 473–496.

Niemes, S., Langhans, M., Viotti, C., Scheuring, D., San Wan Yan, M., Jiang, L., Hillmer, S., Robinson, D.G., and Pimpl, P. (2010). Retromer recycles vacuolar sorting receptors from the trans-Golgi network. Plant J. **61:** 107–121.

Ohno, H., Stewart, J., Fournier, M.C., Bosshart, H., Rhee, I., Miyatake, S., Saito, T., Gallusser, A., Kirchhausen, T., and Bonifacino, J.S. (1995). Interaction of tyrosine-based sorting signals with clathrin-associated proteins. Science **269:** 1872–1875.

Oliviusson, P., Heinzerling, O., Hillmer, S., Hinz, G., Tse, Y.C., Jiang, L., and Robinson, D.G. (2006). Plant retromer, localized to the prevacuolar compartment and microvesicles in *Arabidopsis*, may interact with vacuolar sorting receptors. Plant Cell **18:** 1239–1252.

Otegui, M.S., and Spitzer, C. (2008). Endosomal functions in plants. Traffic **9:** 1589–1598.

Owen, D.J., and Evans, P.R. (1998). A structural explanation for the recognition of tyrosine-based endocytotic signals. Science **282:** 1327–1332.

Palade, G. (1975). Intracellular aspects of the process of protein synthesis. Science **189:** 347–358.

Peyroche, A., Antonny, B., Robineau, S., Acker, J., Cherfils, J., and Jackson, C.L. (1999). Brefeldin A acts to stabilize an abortive ARF-GDP-Sec7 domain protein complex: Involvement of specific residues of the Sec7 domain. Mol. Cell **3:** 275–285.

Pfeffer, S.R. (2007). Unsolved mysteries in membrane traffic. Annu. Rev. Biochem. **76:** 629–645.

Phan, N.Q., Kim, S.J., and Bassham, D.C. (2008). Overexpression of Arabidopsis sorting nexin AtSNX2b inhibits endocytic trafficking to the vacuole. Mol. Plant **1:** 961–976.

Pimpl, P., Hanton, S.L., Taylor, J.P., Pinto-daSilva, L.L., and Denecke, J. (2003). The GTPase ARF1p controls the sequence-specific vacuolar sorting route to the lytic vacuole. Plant Cell **15:** 1242–1256.

Pimpl, P., Taylor, J.P., Snowden, C., Hillmer, S., Robinson, D.G., and Denecke, J. (2006). Golgi-mediated vacuolar sorting of the endoplasmic reticulum chaperone BiP may play an active role in quality control within the secretory pathway. Plant Cell **18:** 198–211.

Seaman, M.N.J. (2005). Recycle your receptors with retromer. Trends Cell Biol. **15:** 68–75.

Shimada, T., Koumoto, Y., Li, L., Yamazaki, M., Kondo, M.,

Nishimura, M., and Hara-Nishimura, I. (2006). AtVPS29, a putative component of a retromer complex, is required for the efficient sorting of seed storage proteins. Plant Cell Physiol. **47:** 1187–1194.

Shiratori, T., Miyatake, S., Ohno, H., Nakaseko, C., Isono, K., Bonifacino, J.S., and Saito, T. (1997). Tyrosine phosphorylation controls internalization of CTLA-4 by regulating its interaction with clathrin-associated adaptor complex AP-2. Immunity **6:** 583–589.

Sohn, E.J., Kim, E.S., Zhao, M., Kim, S.J., Kim, H., Kim, Y.W., Lee, Y.J., Hillmer, S., Sohn, U., Jiang, L., and Hwang, I. (2003). Rha1, an Arabidopsis Rab5 homolog, plays a critical role in the vacuolar trafficking of soluble cargo proteins. Plant Cell **15:** 1057–1070.

Sparkes, I.A., Runions, J., Kearns, A., and Hawes, C. (2006). Rapid, transient expression of fluorescent fusion proteins in tobacco plants and generation of stably transformed plants. Nat. Protoc. **1:** 2019–2025.

Staehelin, L.A., and Moore, I. (1995). The plant Golgi apparatus - Structure, functional organization and trafficking mechanisms. Annu. Rev. Plant Physiol. Plant Mol. Biol. **46:** 261–288.

Tamura, K., Shimada, T., Ono, E., Tanaka, Y., Nagatani, A., Higashi, S.I., Watanabe, M., Nishimura, M., and Hara-Nishimura, I. (2003). Why green fluorescent fusion proteins have not been observed in the vacuoles of higher plants. Plant J. **35:** 545–555.

Toyooka, K., Goto, Y., Asatsuma, S., Koizumi, M., Mitsui, T., and Matsuoka, K. (2009). A mobile secretory vesicle cluster involved in mass transport from the Golgi to the plant cell exterior. Plant Cell **21:** 1212–1229.

Tse, Y.C., Mo, B., Hillmer, S., Zhao, M., Lo, S.W., Robinson, D.G., and Jiang, L. (2004). Identification of multivesicular bodies as prevacuolar compartments in *Nicotiana tabacum* BY-2 cells. Plant Cell **16:** 672–693.

Ueda, T., Uemura, T., Sato, M.H., and Nakano, A. (2004). Functional differentiation of endosomes in Arabidopsis cells. Plant J. **40:** 783–789.

Ueda, T., Yamaguchi, M., Uchimiya, H., and Nakano, A. (2001). Ara6, a plant-unique novel type Rab GTPase, functions in the endocytic pathway of *Arabidopsis thaliana*. EMBO J. **20:** 4730–4741.

Uemura, T., Ueda, T., Ohniwa, R.L., Nakano, A., Takeyasu, K., and Sato, M.H. (2004). Systematic analysis of SNARE molecules in Arabidopsis: Dissection of the post-Golgi network in plant cells. Cell Struct. Funct. **29:** 49–65.

Velten, J., Velten, L., Hain, R., and Schell, J. (1984). Isolation of a dual plant promoter fragment from the Ti plasmid of *Agrobacterium tumefaciens*. EMBO J. **3:** 2723–2730.

Wang, J.Q., Cai, Y., Miao, Y.S., Lam, S.K., and Jiang, L.W. (2009). Wortmannin induces homotypic fusion of plant prevacuolar compartments. J. Exp. Bot. **60:** 3075–3083.

Yamazaki, M., Shimada, T., Takahashi, H., Tamura, K., Kondo, M., Nishimura, M., and Hara-Nishimura, I. (2008). Arabidopsis VPS35, a retromer component, is required for vacuolar protein sorting and involved in plant growth and leaf senescence. Plant Cell Physiol. **49:** 142–156.